Free Radical Homolytic Substitution by the Frontside Mechanism: Ab Initio Study of Homolytic Substitution Reactions at Silicon, Germanium, and Tin

Sonia M. Horvat, Carl H. Schiesser,* and Lisa M. Wild

School of Chemistry, The University of Melbourne, Victoria, Australia 3010

Received November 4, 1999

Ab initio calculations using the 6-311G**, cc-pVDZ, aug-cc-pVDZ, and (valence) double-ζ pseudopotential (DZP) basis sets, with (MP2, QCISD, CCSD(T)) and without (UHF) the inclusion of electron correlation, predict that degenerate homolytic substitution by silyl radical at the silicon atom in disilane can proceed by mechanisms which involve both backside and frontside attack at silicon. At the highest level of theory (CCSD(T)/aug-cc-pVDZ//MP2/aug-cc-pVDZ), energy barriers ($\Delta E^{\ddagger}$) of 52.7 and 58.2 kJ mol^{-1} are calculated for the backside and frontside reactions, respectively. Similar results are obtained at the CCSD(T)/DZP//MP2/DZP level of theory for reactions involving germanium and tin with values of $\Delta E^{\ddagger}$ of 65.2 kJ mol^{-1} (backside) and 76.7 kJ mol^{-1} (frontside) for reactions of germyl radical with digermane and 58.5 kJ mol^{-1} (backside) and 59.1 kJ mol^{-1} (frontside) for reactions of stannyl radical with distannane. CCSD(T)/DZP//MP2/DZP calculations involving the analogous nondegenerate reactions of disilane, digermane, and distannane, as well as reactions involving silylgermane, silylstannane, and germylstannane, predict that while homolytic substitution at silicon and germanium is expected to favor the backside mechanism, reactions involving free-radical attack at tin are predicted to be less discriminate; indeed, in many cases, the frontside mechanism is calculated to be preferred for reactions involving tin. CCSD(T)/DZP//MP2/DZP calculated energy barriers range from 39.4 kJ mol^{-1} for the reaction of silyl radical with distannane by the frontside mechanism to 104.5 kJ mol^{-1} for the analogous frontside reaction involving stannyl radical and disilane. Except for reactions involving attack at the tin atom in methylstannane, we were unable to locate transition states for frontside attack at correlated levels of theory for reactions involving methyl radical. The mechanistic implications of these computational data are discussed.

Downloaded by CARLI CONSORTIUM on June 29, 2009
Published on March 3, 2000 on http://pubs.acs.org | doi: 10.1021/om990886j

Introduction

Intramolecular (1,*n*) group transfer chemistry involving silyl, germyl, and stannyl radicals can be useful in free radical synthesis.[1] Radical Brook-type rearrangements[2] and the 1,5- and 1,6-translocations reported by Kim and co-workers[3] are representative of this chemistry (Scheme 1); other examples can be found in recent reviews.[1,4] Interestingly, while several reports exist of intramolecular homolytic translocations involving group IV elements, we are aware of only one example of a chalcogen-containing group becoming involved in this sort of chemistry[5] and none involving halogen.[1] Why should group IV heteroatoms readily undergo intramolecular homolytic group transfer reactions, while there are so few reports for other systems? The answer to this question almost certainly rests with the intimate details of the homolytic substitution step itself.

Scheme 1

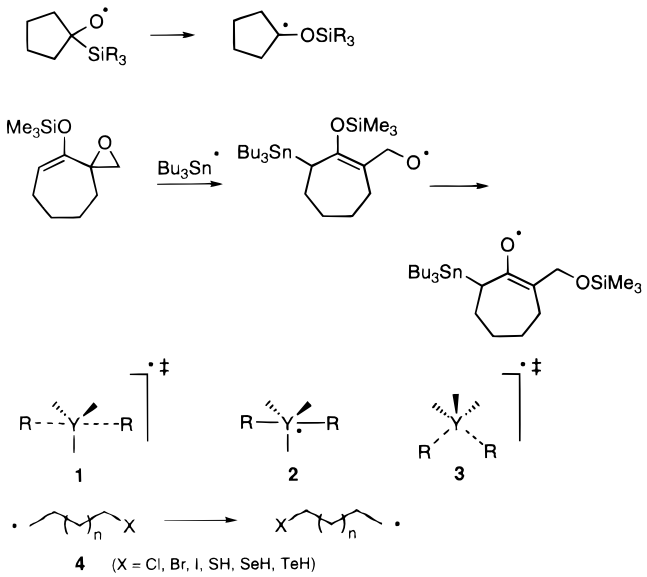

Work in our laboratories has been directed toward the design, application, and understanding of free-radical

(1) Schiesser, C. H.; Wild, L. M. *Tetrahedron* **1996**, *52*, 13256.
(2) (a) Dalton, J. C.; Bourque, R. A. *J. Am. Chem. Soc.* **1981**, *103*, 699. (b) Tsai, Y.-M.; Cherng, C.-D. *Tetrahedron Lett.* **1991**, *32*, 3515.
(3) (a) Kim, S.; Koh, J. S. *J. Chem. Soc. Chem. Commun.* **1992**, 1377. (b) Kim, S.; Lee, S.; Koh, J. S. *J. Am. Chem. Soc.* **1991**, *113*, 5106. (c) Kim, S.; Lim, K. M. *J. Chem. Soc., Chem. Commun.* **1993**, 1152. (d) Kim, S.; Lim, K. M., *Tetrahedron Lett.* **1993**, *34*, 4851. (e) Kim, S.; Do, J. Y.; Lim, K. M. *J. Chem. Soc., Perkin Trans. 1* **1994**, 2517. (f) Kim, S.; Do, J. Y.; Lim, K. M. *Chem. Lett.* **1996**, 669.
(4) Walton, J. C. *Acc. Chem. Res.* **1998**, *31*, 99.
(5) Fong, M. C.; Schiesser, C. H. *Aust. J. Chem.* **1992**, *45*, 475.

10.1021/om990886j CCC: $19.00 © 2000 American Chemical Society
Publication on Web 03/03/2000

Downloaded by CARLI CONSORTIUM on June 29, 2009
Published on March 3, 2000 on http://pubs.acs.org | doi: 10.1021/om990886j

homolytic substitution chemistry with the aim of developing novel synthetic methodology. To that end, we published recently several ab initio studies with the aim of increasing our understanding of the factors which affect and control the mechanism of homolytic substitution at several main-group higher heteroatoms. It is generally agreed that homolytic substitution by a radical ($R^{\bullet}$) at a group (Y) proceeds either via a transition state (**1**) in which the attacking and leaving radicals adopt a collinear (or nearly so) arrangement, resulting in Walden inversion, or with the involvement of a hypervalent intermediate (**2**) which may or may not undergo pseudorotation prior to dissociation.[1] Indeed, high-level ab initio calculations support this view for reactions involving free radical attack at the pnicogens, chalcogens, and halogens; reactions involving phosphorus[6] and tellurium[7] are predicted to involve intermediates, while sulfur,[8,9] selenium,[8−10] and the halogens[11,12] appear to proceed by direct displacement of the leaving radical.

In addition to the translocation chemistry described above, the question of mechanism in homolytic substitution chemistry involving tetravalent silicon, germanium, and tin is of topical interest in polymer chemistry; it would appear that intramolecular homolytic substitution at tetravalent silicon plays an important role in radical-based degradation of poly(phenylsilane).[13] If one considers carefully the pathways available for homolytic free-radical attack at higher heteroatoms, it seems reasonable to suggest a pathway involving frontside attack via transition state **3** in addition to those already discussed. Indeed, Dobbs and Doren explored the mechanism of the reaction of hydrogen atom with disilane and noted that frontside homolytic substitution is more favorable than the analogous backside mechanism by 11.7 kJ mol^{-1} at the MP2/6-311G** level of theory.[14] This value correlates well with available experimental data.[15]

We recently explored this mechanism by computational techniques for 1,*n*-translocations of halogens and chalcogens in ω-haloalkyl and ω-chalcogenylalkyl radicals (**4**) and concluded frontside displacement to be an unlikely pathway for these elements.[9,12] On the other hand, similar computational investigations into the mechanism of the radical Brook rearrangement concluded that 1,2-migrations involving group IV elements proceeded via the frontside homolytic substitution mechanism.[16]

To explore further trends within the main-group higher heteroatoms, we now report the results of computational investigations into the frontside and backside mechanisms for free radical homolytic substitution by silyl (SiH_3), germyl (GeH_3), and stannyl (SnH_3) radicals at the heteroatom in disilane (H_3SiSiH_3), digermane (H_3GeGeH_3), distannane (H_3SnSnH_3), silylgermane (H_3SiGeH_3), silylstannane (H_3SiSnH_3), and germylstannane (H_3GeSnH_3). In addition, a computational investigation into the free radical attack of methyl radical at the heteroatom in methylsilane, germane, and stannane by the frontside mechanism is also presented and represents an extension of our previous work in which we explored the requirements of backside attack in these same reactions.[17]

Methods

Ab initio molecular orbital calculations were performed on DEC AlphaStation 400 4/233, Alphaserver 8400, Personal Workstation 433au or 600au, Compaq DS10, or Cray J916 computers using the Gaussian 94[18] system of programs. Geometry optimizations were performed using standard gradient techniques at the SCF, MP2, and B3LYP levels of theory using restricted (RHF, RMP2, RB3LYP) and unrestricted (UHF, UMP2, UB3LYP) methods for closed- and open-shell systems, respectively. Standard basis sets were used, and the (valence) double-ζ pseudopotential basis sets of Hay and Wadt[19] supplemented with a single set of d-type polarization functions were used for the heteroatoms in this study (exponents $d(\zeta)_{Si} = 0.284$,[20] $d(\zeta)_{Ge} = 0.230$,[20] and $d(\zeta)_{Sn} = 0.200$), while the double-ζ all-electron basis sets of Dunning[21] with an additional set of polarization functions (exponents $d(\zeta)_C = 0.75$ and $p(\zeta)_H = 1.00$) were used for C and H. We refer to this basis set as DZP throughout this work.[8,9,11,12,16,17,22] In previous work, results generated using DZP proved to be very similar to those obtained using 6-311G** for reactions involving chlorine and silicon.[12,16,17]

All ground and transition states were verified by vibrational frequency analysis. Further single-point QCISD and CCSD(T) calculations were performed on all MP2 optimized structures. Values of $\langle S^2 \rangle$ never exceeded 0.86 before annihilation of quartet contamination and were mostly below 0.79 at correlated levels of theory. Zero-point vibrational energy corrections have been applied wherever possible.

(6) (a) Schiesser, C. H.; Wild, L. M. *Aust. J. Chem.* **1995**, *48*, 175. See also: (b) Howell, J. M.; Olsen, J. F. *J. Am. Chem. Soc.* **1976**, *98*, 7119. (c) Cramer, C. J. *J. Am. Chem. Soc.* **1990**, *112*, 7965. (d) Cramer, C. J. *J. Am. Chem. Soc.* **1991**, *113*, 2439.

(7) (a) Ferris, K. F.; Franz, J. A.; Sosa, C.; Bartlett, R. J. *J. Org. Chem.* **1992**, *57*, 777. (b) Lyons, J. E.; Schiesser, C. H. *J. Chem. Soc., Perkin Trans. 2* **1992**, 1655.

(8) (a) Smart, B. A.; Schiesser, C. H. *J. Chem. Soc., Perkin Trans. 2* **1994**, 2269. (b) Schiesser, C. H.; Smart, B. A. *Tetrahedron* **1995**, *51*, 6051. (c) Schiesser, C. H.; Smart, B. A.; Tran, T.-A. *Tetrahedron* **1995**, *51*, 10651. (d) Schiesser, C. H.; Smart, B. A. *J. Comput. Chem.* **1995**, *16*, 1055. (e) Schiesser, C. H.; Skidmore, M. A. *Chem. Commun.* **1996**, 1419. (f) Schiesser, C. H.; Skidmore, M. A. *J. Organomet. Chem.* **1998**, *552*, 145.

(9) Schiesser, C. H.; Wild. L. M. *J. Org. Chem.* **1999**, *64*, 1131.

(10) Lyons, J. E.; Schiesser, C. H. *J. Organomet. Chem.* **1992**, *437*, 165.

(11) Schiesser, C. H.; Smart, B. A.; Tran, B.-A. *Tetrahedron* **1995**, *51*, 3327.

(12) Schiesser, C. H.; Wild, L. M. *J. Org. Chem.* **1998**, *63*, 670.

(13) Chatgilialoglu, C.; Barbieri, A. Manuscript in preparation.

(14) Dobbs, K. D.; Doren, D. J. *J. Am. Chem. Soc.* **1993**, *115*, 3731.

(15) Fabry, L.; Potzinger, P.; Reimann, B.; Ritter, A.; Steenberger, H. P. *Organometallics* **1986**, *5*, 1231.

(16) Schiesser, C. H.; Styles, M. L. *J. Chem. Soc., Perkin Trans. 2* **1997**, 2335.

(17) Schiesser, C. H.; Styles, M. L.; Wild, L. M. *J. Chem. Soc., Perkin Trans. 2* **1996**, 2257.

(18) Frisch, M. J.; Trucks, G. W.; Schlegel, H. B.; Gill, P. M. W.; Johnson, B. G.; Robb, M. A.; Cheeseman, J. R.; Keith, T.; Petersson, G. A.; Montgomery, J. A.; Raghavachari, K.; Al-Laham, M. A.; Zakrzewski, V. G.; Ortiz, J. V.; Foresman, J. B.; Peng, C. Y.; Ayala, P. Y.; Chen, W.; Wong, M. W.; Andres, J. L.; Replogle, E. S.; Gomperts, R.; Martin, R. L.; Fox, D. J.; Binkley, J. S.; Defrees, D. J.; Baker, J.; Stewart, J. J. P.; Head-Gordon, M.; Gonzalez, C.; Pople, J. A. Gaussian 94, Revision B.3; Gaussian Inc., Pittsburgh, PA, 1995.

(19) (a) Wadt, W. R.; Hay, P. J. *J. Chem. Phys.* **1985**, *82*, 284. (b) Hay, P. J.; Wadt, W. R. *J. Chem. Phys.* **1985**, *82*, 270. (c) Hay, P. J.; Wadt, W. R. *J. Chem. Phys.* **1985**, *82*, 299.

(20) Höllwarth, A.; Böhme, M.; Dapprich, S.; Ehlers, A. W.; Gobbi, A.; Jonas, V.; Köhler, K. F.; Stegmann, R.; Veldkamp, A.; Frenking, G. *Chem. Phys. Lett.* **1993**, *208*, 237

(21) Dunning, T. H.; Hay, P. J. *Modern Theoretical Chemistry*; Plenum: New York, 1976; Chapter 1, pp 1−28.

(22) (a) Dakternieks, D.; Henry, D. J.; Schiesser, C. H. *J. Chem. Soc., Perkin Trans. 2* **1997**, 1665. (b) Dakternieks, D.; Henry, D. J.; Schiesser, C. H. *J. Chem. Soc., Perkin Trans. 2* **1998**, 591. (c) Dakternieks, D.; Henry, D. J.; Schiesser, C. H. *Organometallics* **1998**, *17*, 1079.

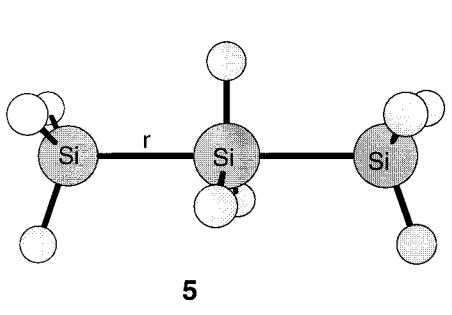

5

	r
MP2/6-311G**	2.504Å
MP2/DZP	2.472Å
MP2/cc-pVDZ	2.534Å
MP2/aug-cc-pVDZ	2.534Å
B3LYP/6-311G**	2.536Å
B3LYP/DZP	2.480Å

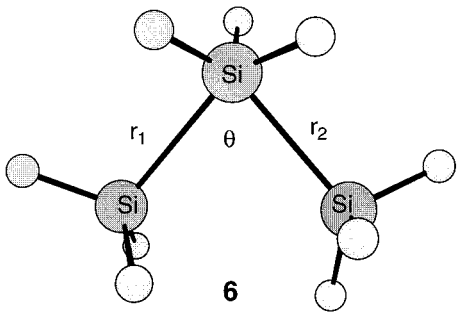

6

	r1	r2	θ
MP2/6-311G**	2.465Å	2.531Å	81.2°
MP2/DZP	2.470Å	2.503Å	81.0°
MP2/cc-pVDZ	2.499Å	2.545Å	80.5°
MP2/aug-cc-pVDZ	2.533Å	2.548Å	79.8°
B3LYP/6-311G**	2.487Å	2.548Å	83.5°
B3LYP/DZP	2.480Å	2.526Å	83.5°

Figure 1. Optimized structures of transition states **5** and **6** for the degenerate backside and frontside reactions of silyl radical ($^{\bullet}SiH_3$) with disilane (H_3SiSiH_3).

Downloaded by CARLI CONSORTIUM on June 29, 2009
Published on March 3, 2000 on http://pubs.acs.org | doi: 10.1021/om990886j

Scheme 2

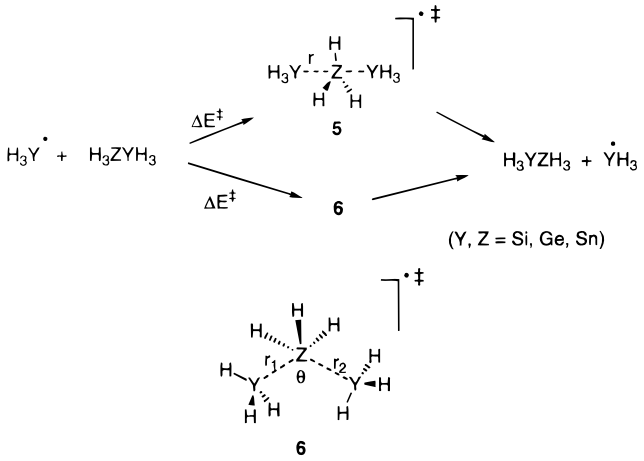

Results and Discussion

Reaction of Silyl Radical with Disilane, Germyl Radical with Digermane, and Stannyl Radical with Distannane. Extensive searching of the Si_3H_9 potential energy surface at the UHF/6-311G**, MP2/6-311G**, MP2/DZP, MP2/cc-pVDZ, MP2/aug-cc-pVDZ, and B3LYP/6-311G** levels of theory located structures **5** and **6** (Y, Z = Si) as transition states for the degenerate homolytic substitution by the silyl radical at disilane. The important geometric features of structures **5** and **6** (Y, Z = Si) are summarized in Figure 1, while calculated energy barriers ($\Delta E^{\ddagger}$; Scheme 2) are listed in Table 1 together with the calculated imaginary frequency corresponding to structures **5** and **6**. Full computational details are available as Supporting Information.

Inspection of Figure 1 reveals that while the transition state **5** for backside attack is predicted to adopt an exactly collinear arrangement of attacking and leaving radicals at all levels of theory employed, structure **6** involved in the analogous frontside chemistry is predicted to involve an attack angle of around 80° at all levels of theory and resembles strongly the structures predicted to be involved in the 1,2-homolytic translocations of silyl groups.[16] Transition state (Si−Si) separations in both **5** and **6** (Y, Z = Si) are predicted to lie between 2.465 and 2.548 Å at all levels of theory.

This computational study also suggests that the energy requirements for both homolytic pathways are similar. Inspection of Table 1 reveals that, as expected, electron correlation is important in achieving reliable values for $\Delta E^{\ddagger}$. HF/6-311G** calculations predict energy barriers of 119.2 and 125.5 kJ mol^{-1} for reactions involving **5** and **6**, respectively. Inclusion of electron correlation (MP2/6-311G**) serves to lower these barriers to 72.0 and 79.5 kJ mol^{-1}, respectively, while inclusion of zero-point vibrational energy correction (ZPE) would appear to have only a minor effect on the calculated energy barriers in question. Further improvements in both basis set quality and correlation provide values of $\Delta E^{\ddagger}$ for the reaction involving **5** of 55.6 (MP2/aug-cc-pVDZ), 74.1 (QCISD/6-311G**//MP2/6-311G**), and 60.7 kJ mol^{-1} (QCISD/aug-cc-pVDZ//MP2/aug-cc-pVDZ). In comparison, reactions involving **6** are calculated to have $\Delta E^{\ddagger}$ values of 63.2 (MP2/aug-cc-pVDZ), 80.3 (QCISD/6-311G**//MP2/6-311G**), and 66.1 kJ mol^{-1} (QCISD/aug-cc-pVDZ//MP2/aug-cc-pVDZ). At the highest level of theory used (CCSD(T)/aug-cc-pVDZ//MP2/aug-cc-pVDZ), energy barriers ($\Delta E^{\ddagger}$) of 52.7 and 58.2 kJ mol^{-1} are predicted for the pathways involving **5** and **6**, respectively, while values of 44.4 and 60.7 kJ mol^{-1} are obtained at the B3LYP/6-311G** level. Clearly, both backside and frontside mechanisms are predicted to be feasible for homolytic substitution by a silyl radical at a tetravalent silicon atom. This is a significant result because it represents a rare example of a frontside transition state located for an intermolecular homolytic substitution reaction. The similarities in activation energy for both pathways suggest that, depending on the geometric requirements, homolytic substitution at a tetravalent silicon atom in general may well involve either or both of the mechanisms discussed. It is interesting to note the disparity between the B3LYP and other data listed in Table 1, the density functional method providing a 2−3-fold increase in the calculated difference in values for $\Delta E^{\ddagger}$ for the frontside and backside attack mechanisms than the other methods

Table 1. Calculated Energy Barriers[a] ($\Delta E^{\ddagger}$) for the Degenerate Reactions of Silyl (SiH_3), Germyl (GeH_3), and Stannyl (SnH_3) Radicals with Disilane (H_3SiSiH_3), Digermane (H_3GeGeH_3), and Distannane (H_3SnSnH_3) (Scheme 2; Y = Z = Si, Ge, Sn) and Transition State (Imaginary) Frequencies (ν)[b] of Structures 5 and 6

			5			6		
Y	Z	method	$\Delta E^{\ddagger}$	$\Delta E^{\ddagger}$ + ZPE	ν	$\Delta E^{\ddagger}$	$\Delta E^{\ddagger}$ + ZPE	ν
Si	Si	HF/6-311G**	119.2	120.0	1050i	125.5	130.5	453i
		HF/DZP	124.5	125.3	1030i	131.6	135.5	470i
		MP2/6-311G**	72.0	72.4	442i	79.5	82.8	347i
		MP2/DZP	70.6	72.3	384i	82.4	86.2	371i
		MP2/cc-pVDZ	65.3	66.1	287i	74.9	78.2	358i
		MP2/aug-cc-pVDZ	55.6	56.9	106i	63.2	66.5	352i
		QCISD/6-311G**//MP2/6−311G**	74.1			80.3		
		QCISD/DZP//MP2/DZP	71.3			81.7		
		QCISD/cc-pVDZ//MP2/cc-pVDZ	62.3			70.3		
		QCISD/aug-cc-pVDZ//MP2/aug-cc-pVDZ	60.7			66.1		
		CCSD(T)/6-311G**//MP2/6−311G**	67.5			73.7		
		CCSD(T)/DZP//MP2/DZP	65.2			75.8		
		CCSD(T)/cc-pVDZ//MP2/cc-pVDZ	62.3			70.3		
		CCSD(T)/aug-cc-pVDZ//MP2/aug-cc-pVDZ	52.7			58.2		
		B3LYP/6-311G**	44.4	45.6	380i	60.7	63.6	286i
		B3LYP/DZP	51.2	52.4	414i	65.5	68.4	299i
Ge	Ge	HF/DZP	118.4	118.3	893i	126.3	128.2	365i
		MP2/DZP	70.7	71.5	398i	83.7	85.8	328i
		QCISD/DZP//MP2/DZP	70.9			82.7		
		CCSD(T)/DZP//MP2/DZP	65.2			76.7		
		B3LYP/DZP	50.0	52.4	351i	66.9	68.5	250i
Sn	Sn	HF/DZP	106.0	104.9	915i	99.8	101.1	285i
		MP2/DZP	65.1	65.7	426i	66.0	68.2	266i
		QCISD/DZP//MP2/DZP	63.0			63.2		
		CCSD(T)/DZP//MP2/DZP	58.5			59.1		
		B3LYP/DZP	42.1	41.7	332i	49.5	50.3	189i

[a] Energies in kJ mol^{-1}. [b] Frequencies in cm^{-1}.

Downloaded by CARLI CONSORTIUM on June 29, 2009
Published on March 3, 2000 on http://pubs.acs.org | doi: 10.1021/om990886j

utilized. We have previously noted irregularities between density-functional methods and other ab initio techniques when applied to some free radical reactions.[23]

There are some considerable computational issues that need to be addressed in performing all-electron ab initio calculations on molecules containing higher heteroatoms such as tin, especially when electron correlation is required.[16,17,22] To alleviate resource problems, we have chosen to perform calculations utilizing a polarization double-ζ pseudopotential basis set (DZP). In previous work, this basis set has provided data similar to those produced using 6-311G** and, as such, we felt that, at the very least, a good qualitative picture for many reactions involving higher heteroatoms could be established through the use of DZP.[8,9,11,12,16,17,22] In this current work, the data presented in Table 1 indicate clearly that CCSD(T)/DZP//MP2/DZP calculations provide values for $\Delta E^{\ddagger}$ which are about 12 kJ mol^{-1} larger than those predicted at the highest level of theory for the reactions of silyl radical with disilane. With this in mind, together with the knowledge that all correlated levels of theory provide a difference in the values of $\Delta E^{\ddagger}$ for reactions involving **5** and **6** ($\Delta E^{\ddagger}$(**6**) − $\Delta E^{\ddagger}$(**5**)) of between 5.5 and 7.9 kJ mol^{-1}, we were confident that similar DZP calculations involving the remaining systems in this study would provide useful information about the mechanism of homolytic substitution chemistry involving silicon, germanium, and tin.

Searching of the Ge_3H_9 and Sn_3H_9 potential energy surfaces at the UHF/DZP, MP2/DZP, and B3LYP/DZP levels of theory located transition states **5** and **6** (Y = Z = Ge, Sn). These structures bear a striking resemblance to the analogous silicon transition states **5** and **6** (Y = Z = Si), and their important geometric features are listed in Table 2, while the calculated energy barriers ($\Delta E^{\ddagger}$; Scheme 2) are listed in Table 1 together with the calculated imaginary frequency corresponding to structures **5** and **6**. Full structural details are

Table 2. UHF/DZP, MP2/DZP, and B3LYP/DZP Calculated Important Geometric Features[a] of the Transition Structures 5 and 6 Involved in the Degenerate Reactions of Silyl (SiH_3) Germyl (GeH_3), and Stannyl (SnH_3) Radicals with Digermane (H_3GeGeH_3), Distannane (H_3SnSnH_3), Silylgermane (H_3SiGeH_3), Silylstannane (H_3SiSnH_3), and Germylstannane (H_3GeSnH_3) (Scheme 2)

			5	6		
Y	Z	method	r	r_1	r_2	θ
Ge	Ge	UHF/DZP	2.758	2.732	2.774	79.2
		MP2/DZP	2.689	2.657	2.682	79.0
		B3LYP/DZP	2.720	2.673	2.713	81.3
Sn	Sn	UHF/DZP	3.105	3.100	3.133	77.4
		MP2/DZP	3.039	3.029	3.044	76.5
		B3LYP/DZP	3.066	3.042	3.072	79.1
Si	Ge	UHF/DZP	2.673	2.633	2.678	79.4
		MP2/DZP	2.605	2.561	2.592	79.4
		B3LYP/DZP	2.636	2.573	2.617	81.9
Si	Sn	UHF/DZP	2.827	2.819	2.869	75.9
		MP2/DZP	2.763	2.753	2.780	74.7
		B3LYP/DZP	2.789	2.756	2.801	78.3
Ge	Si	UHF/DZP	2.663	2.634	2.676	80.7
		MP2/DZP	2.599	2.568	2.594	80.7
		B3LYP/DZP	2.629	2.581	2.622	82.9
Ge	Sn	UHF/DZP	2.906	2.902	2.952	76.1
		MP2/DZP	2.842	2.837	2.861	74.7
		B3LYP/DZP	2.868	2.844	2.885	78.0
Sn	Si	UHF/DZP	2.889	2.858	2.882	81.5
		MP2/DZP	2.814	2.777	2.790	81.8
		B3LYP/DZP	2.847	2.800	2.826	83.4
Sn	Ge	UHF/DZP	2.975	2.948	2.972	80.1
		MP2/DZP	2.896	2.859	2.873	80.3
		B3LYP/DZP	2.929	2.885	2.910	82.0

[a] Distances in Å and angles in deg.

(23) Morihovitis, T.; Schiesser, C. H.; Skidmore, M. A. *J. Chem. Soc., Perkin Trans. 2* **1999**, 2041.

Table 3. Calculated Energy Barriers[a] ($\Delta E^{\ddagger}$) for the Degenerate Reactions of Silyl (SiH_3), Germyl (GeH_3), and Stannyl (SnH_3) Radicals with Silylgermane (H_3SiGeH_3), Silylstannane (H_3SiSnH_3), and Germylstannane (H_3GeSnH_3) (Scheme 2; Y ≠ Z) and Transition State (Imaginary) Frequencies (ν)[b] of Structures 5 and 6

			5			6		
Y	Z	method	$\Delta E^{\ddagger}$	$\Delta E^{\ddagger}$ + ZPE	ν	$\Delta E^{\ddagger}$	$\Delta E^{\ddagger}$ + ZPE	ν
Si	Ge	HF/DZP	124.4	124.8	929i	129.2	132.5	424i
		MP2/DZP	72.9	74.6	388i	83.4	86.7	352i
		QCISD/DZP//MP2/DZP	72.2			81.5		
		CCSD(T)/DZP//MP2/DZP	66.1			75.6		
		B3LYP/DZP	53.2	54.3	365i	66.3	68.8	276i
Si	Sn	HF/DZP	111.9	112.3	1037i	101.4	105.0	359i
		MP2/DZP	64.4	66.3	322i	63.1	67.2	301i
		QCISD/DZP//MP2/DZP	61.5			59.7		
		CCSD(T)/DZP//MP2/DZP	55.4			54.3		
		B3LYP/DZP	39.0	40.3	215i	44.6	47.3	215i
Ge	Si	HF/DZP	120.1	120.1	1005i	130.6	133.3	437i
		MP2/DZP	69.8	70.4	428i	84.8	87.4	369i
		QCISD/DZP//MP2/DZP	71.2			84.6		
		CCSD(T)/DZP//MP2/DZP	65.4			78.9		
		B3LYP/DZP	49.4	49.8	417i	68.0	69.9	290i
Ge	Sn	HF/DZP	108.4	108.1	995i	99.5	102.0	295i
		MP2/DZP	63.8	64.6	336i	63.1	65.9	264i
		QCISD/DZP//MP2/DZP	62.0			60.6		
		CCSD(T)/DZP//MP2/DZP	56.2			55.5		
		B3LYP/DZP	38.3	38.8	307i	45.5	47.6	186i
Sn	Si	HF/DZP	116.4	115.2	952i	130.2	131.3	442i
		MP2/DZP	72.9	73.2	528i	89.6	91.5	401i
		QCISD/DZP//MP2/DZP	73.4			88.5		
		CCSD(T)/DZP//MP2/DZP	69.0			84.0		
		B3LYP/DZP	57.9	51.9	460i	72.8	73.2	309i
Sn	Ge	HF/DZP	114.1	113.2	842i	125.4	126.1	365i
		MP2/DZP	72.2	72.8	461i	87.1	88.6	349i
		QCISD/DZP//MP2/DZP	71.8			85.1		
		CCSD(T)/DZP//MP2/DZP	67.4			80.6		
		B3LYP/DZP	52.6	52.0	389i	70.6	70.7	259i

[a] Energies in kJ mol^{-1}. [b] Frequencies in cm^{-1}.

Downloaded by CARLI CONSORTIUM on June 29, 2009
Published on March 3, 2000 on http://pubs.acs.org | doi: 10.1021/om990886j

available as Supporting Information. Backside attack structures (**5**) are calculated to adopt a collinear arrangement of attacking and leaving radicals, while the frontside structures (**6**) are predicted to involve attack angles of about 79° (Ge) to 77° (Sn). Once again, regardless of mechanism, the transition state distances are calculated to lie in narrow ranges of 2.65−2.77 Å (Ge) and 3.02−3.13 Å (Sn). The calculated energy barriers ($\Delta E^{\ddagger}$) for the reactions involving germanium range from 65.2 (CCSD(T)/DZP//MP2/DZP) to 118.4 kJ mol^{-1} (HF/DZP) for the reaction involving **5**, while similar barriers for the reaction involving **6** are calculated to range from 76.7 (CCSD(T)/DZP//MP2/DZP) to 126.3 kJ mol^{-1} (HF/DZP). Similar trends are predicted for reactions involving tin, with barriers of 58.5 and 59.1 kJ mol^{-1} predicted at the highest level for backside and frontside attack mechanisms, respectively.

These data are to be compared with previous values calculated for the reactions involving silicon. It would seem that not only are reactions involving tin calculated to be the most facile, they are also calculated to be the least discriminate, with a difference of only 0.6 kJ mol^{-1} calculated for pathways involving **5** and **6**.

Degenerate Reactions of Silyl, Germyl, and Stannyl Radicals with Silylgermane, Silylstannane, and Germylstannane. We next turned our attention to similar degenerate reactions involving H_3SiGeH_3, H_3SiSnH_3, and H_3GeSnH_3. Once again, transition states **5** and **6** were located for the backside and frontside attack mechanisms (Scheme 2) and selected geometric data are listed in Table 2, while the calculated energy barriers ($\Delta E^{\ddagger}$) are listed in Table 3; full details are available as Supporting Information. Once again, transition states **5** are calculated to adopt a collinear arrangement of attacking and leaving radicals, while the analogous frontside structures **6** adopt attack angles of between about 74 and 83°, depending on the element undergoing homolytic substitution and the level of theory employed. Attack distances are, once again, very similar for both the frontside and backside structures (**5** and **6**) for a given arrangement of elements, with Si−Ge, Si−Sn, and Ge−Sn separations of about 2.56−2.69, 2.75−2.89, and 2.84−2.97 Å, respectively.

Some interesting trends in energy are clearly evident upon inspection of Table 3. Calculated energy barriers ($\Delta E^{\ddagger}$) are once again affected strongly by the inclusion of electron correlation. At any given level of theory, it is clear that values of $\Delta E^{\ddagger}$ are dependent on the nature of the atom undergoing homolytic substitution and the attacking/leaving radical. As observed in previous work,[16,17] for given attacking and leaving species, the order of reactivity is calculated to be Sn > Si ≥ Ge. For example, at the highest level of theory (CCSD(T)/DZP//MP2/DZP) values of 66.1 and 55.4 kJ mol^{-1} are calculated for the backside attack of silyl radical at the germanium and tin atoms in silylgermane and silylstannane, respectively. These numbers are to be compared with the value of 65.2 kJ mol^{-1} (Table 1) for the analogous attack at disilane at the same level of theory. The similar data for the analogous reactions involving **6** are 75.8 (Si), 75.6 (Ge), and 54.3 (Sn) kJ mol^{-1}. In addition, for a given element undergoing homolytic attack, the attack of silyl radical is predicted to be more

facile than the reaction of germyl radical, which, in turn, is predicted to be more reactive than stannyl radical, observations also consistent with previous observations.[8,11] For example, energy barriers ($\Delta E^{\ddagger}$) of 55.4, 56.2, and 58.5 kJ mol^{-1} are calculated for the backside attack of silyl, germyl, and stannyl radicals, respectively, at the tin atom with expulsion of another molecule of the attacking species.

More interesting are the predicted trends vis-à-vis the question of frontside versus backside attack mechanism. The data presented in Tables 1 and 3 suggest that while at all levels of theory both mechanisms are feasible, the backside mechanism, involving transition state **5**, is favored by 12−15 kJ mol^{-1} for attack at silicon and by 9−13 kJ mol^{-1} for attack at germanium, while attack at tin is calculated be essentially indiscriminate. Indeed, attack of silyl radical at the tin atom in silylstannane is predicted to slightly favor the frontside mechanism at all levels of theory; CCSD(T)/DZP//MP2/DZP calculations predict that **6** (Y = Si, Z = Sn) is favored over **5** (Y = Si, Z = Sn) by 1.1 kJ mol^{-1}. Similarly, **6** (Y = Ge, Z = Sn) is favored over **5** (Y = Ge, Z = Sn) by 0.7 kJ mol^{-1} at the same level of theory.

Nondegenerate Reactions of Silyl, Germyl and Stannyl Radicals with Silylgermane, Silylstannane, and Germylstannane. Transition states **7** and **8** for the remaining, nondegenerate reactions of silyl, germyl, and stannyl radicals with silylgermane, silylstannane, and germylstannane were located at the same levels of theory used for the previous reactions in this study. Important structural features are listed in Table

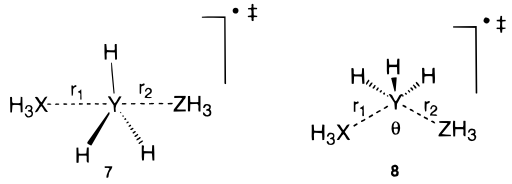

4. The calculated energy barriers for the forward ($\Delta E^{\ddagger}_1$) and reverse ($\Delta E^{\ddagger}_2$) reactions (Scheme 3) are listed in Table 5 together with the (imaginary) transition state frequency where calculated. Not surprisingly, the data presented in Table 5 show trends similar to those found in Tables 1 and 3. Specifically, lower energy barriers ($\Delta E^{\ddagger}_1$, $\Delta E^{\ddagger}_2$) are predicted when the attacking species is silyl radical, when the leaving moiety is stannyl radical, and when the center undergoing homolytic attack is tin. At the CCSD(T)/DZP//MP2/DZP level of theory, the highest energy barrier (104.5 kJ mol^{-1}) is calculated to be that for the frontside attack of stannyl radical at silylstannane with expulsion of silyl radical, while the lowest barrier is calculated to be 39.4 kJ mol^{-1} and corresponds to the frontside attack of silyl radical at distannane with expulsion of stannyl radical.

These trends are also evident in the geometries of transition states **7** and **8**, in which lower barriers, as expected, are found to correspond to "earlier" structures. For example, the data presented in Table 5 reveal that the MP2/DZP calculated transition state silicon−germanium separation in **7** steadily increases as the leaving group moves from silyl radical (2.605 Å) to germyl (2.648 Å) and stannyl (2.700 Å). These reactions, in turn, are accompanied by steady decreases in activation energy (66.1, 56.4, 47.8 kJ mol^{-1}). The similar data

Table 4. UHF/DZP, MP2/DZP, and B3LYP/DZP Calculated Important Geometric Features[a] of the Transition Structures 7 and 8 Involved in the Nondegenerate Reactions of Silyl (SiH_3) Germyl (GeH_3), and Stannyl (SnH_3) Radicals with Digermane (H_3GeGeH_3), Distannane (H_3SnSnH_3), Silylgermane (H_3SiGeH_3), Silylstannane (H_3SiSnH_3), and Germylstannane (H_3GeSnH_3) (Scheme 3)

				7		**8**		
X	Y	Z	method	r_1	r_2	r_1	r_2	θ
Si	Si	Ge	UHF/DZP	2.560	2.642	5.549	2.659	81.1
			MP2/DZP	2.568	2.556	2.483	2.579	81.4
			B3LYP/DZP	2.597	2.586	2.492	2.608	83.5
Si	Si	Sn	UHF/DZP	2.644	2.830	2.571	2.829	82.4
			MP2/DZP	2.629	2.728	2.496	2.751	83.1
			B3LYP/DZP	2.679	2.752	2.527	2.764	84.7
Si	Ge	Ge	UHF/DZP	2.693	2.738	2.756	2.648	79.7
			MP2/DZP	2.648	2.652	2.666	2.574	79.8
			B3LYP/DZP	2.678	2.684	2.699	2.585	81.9
Si	Ge	Sn	UHF/DZP	2.731	2.924	2.667	2.925	80.8
			MP2/DZP	2.698	2.821	2.587	2.833	81.6
			B3LYP/DZP	2.739	2.850	2.616	2.854	83.1
Si	Sn	Ge	UHF/DZP	2.841	2.891	2.823	2.943	76.4
			MP2/DZP	2.799	2.811	2.760	2.850	75.4
			B3LYP/DZP	2.822	2.838	2.760	2.880	78.6
Si	Sn	Sn	UHF/DZP	2.863	3.071	2.843	3.101	77.5
			MP2/DZP	2.831	2.980	2.780	3.005	77.4
			B3LYP/DZP	2.869	3.000	2.794	3.022	80.1
Ge	Si	Sn	UHF/DZP	2.704	2.849	2.642	2.867	82.0
			MP2/DZP	2.668	2.754	2.570	2.782	82.2
			B3LYP/DZP	2.702	2.785	2.586	2.817	83.9
Ge	Ge	Sn	UHF/DZP	2.792	2.941	2.738	2.961	80.5
			MP2/DZP	2.744	2.846	2.659	2.864	80.6
			B3LYP/DZP	2.775	2.880	2.678	2.902	82.5
Ge	Sn	Sn	UHF/DZP	2.926	3.085	2.899	3.136	77.5
			MP2/DZP	2.886	2.999	2.837	3.039	76.6
			B3LYP/DZP	2.910	3.026	2.840	3.074	79.5

[a] Distances in Å and angles in deg.

Scheme 3

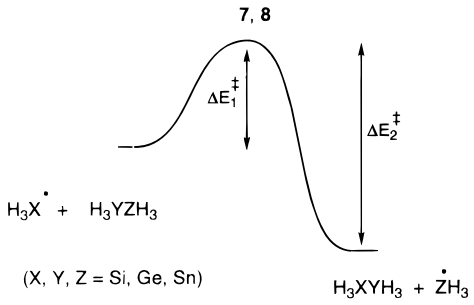

for **8** are silyl (2.561 Å) < germyl (2.666 Å) < stannyl (2.833 Å), with corresponding energy barriers of 75.6, 66.3, and 56.6 kJ mol^{-1}, respectively.

Once again, the data in Table 3 reveal a slight preference for homolytic substitution at a tin center to follow a frontside attack mechanism as opposed to a backside mechanism, the largest preference being only 2.0 kJ mol^{-1}. In general, however, substitution at tin would be expected to proceed by both mechanisms, while the analogous reactions at silicon and germanium are predicted to have a preference for the backside mechanism, with the degree of preference dependent on the system in question. In no system in this study is the difference in activation energy for the two mechanisms sufficiently large to rule out one mechanism completely. One might expect, therefore, that depending on substitution and geometric constraints in systems of experi-

Downloaded by CARLI CONSORTIUM on June 29, 2009
Published on March 3, 2000 on http://pubs.acs.org | doi: 10.1021/om990886j

Table 5. Calculated Energy Barriers[a] ($\Delta E^{\ddagger}$) for the Nondegenerate Reactions of Silyl (SiH_3), Germyl (GeH_3), and Stannyl (SnH_3) Radicals with Silylgermane (H_3SiGeH_3), Silylstannane (H_3SiSnH_3), and Germylstannane (H_3GeSnH_3) (Scheme 3) and Transition State (Imaginary) Frequencies (ν)[b] of Structures 7 and 8

				7					8				
X	Y	Z	method	$\Delta E_1^{\ddagger}$	$\Delta E_1^{\ddagger}$ + ZPE	$\Delta E_2^{\ddagger}$	$\Delta E_2^{\ddagger}$ + ZPE	ν	$\Delta E_1^{\ddagger}$	$\Delta E_1^{\ddagger}$ + ZPE	$\Delta E_2^{\ddagger}$	$\Delta E_2^{\ddagger}$ + ZPE	ν
Si	Si	Ge	HF/DZP	113.4	114.4	131.8	131.6	1013i	121.5	125.2	139.9	142.5	429i
			MP2/DZP	60.7	62.2	82.0	82.3	554i	72.6	76.3	93.9	96.4	342i
			QCISD/DZP[c]	60.6		82.6			72.0		93.9		
			CCSD(T)/DZP[d]	54.8		76.9			66.1		88.2		
			B3LYP/DZP	41.0	42.4	61.1	61.4	407i	56.2	59.0	76.3	78.0	265i
Si	Si	Sn	HF/DZP	100.9	102.1	143.9	142.3	962i	108.6	112.1	151.6	152.2	392i
			MP2/DZP	52.2	53.9	101.1	100.7	610i	60.6	63.8	109.5	110.5	258i
			QCISD/DZP[c]	51.2		100.1			60.3		109.1		
			CCSD(T)/DZP[d]	45.8		95.7			54.6		104.5		
			B3LYP/DZP	32.6	34.3	79.4	78.3	391i	44.8	47.5	91.6	91.5	197i
Si	Ge	Ge	HF/DZP	113.3	114.1	129.7	129.3	908i	119.2	122.4	135.6	137.6	372i
			MP2/DZP	63.1	64.8	82.0	82.4	482i	73.8	77.1	92.7	94.7	313i
			QCISD/DZP[c]	62.2		81.5			72.1		91.4		
			CCSD(T)/DZP[d]	56.4		75.8			66.3		85.6		
			B3LYP/DZP	42.9	44.4	61.0	61.3	357i	57.1	59.7	75.2	76.5	232i
Si	Ge	Sn	HF/DZP	102.2	103.5	138.5	136.9	868i	108.6	111.5	144.8	145.0	342i
			MP2/DZP	55.0	56.8	97.0	96.7	552i	63.5	66.4	105.6	106.3	250i
			QCISD/DZP[c]	53.3		95.1			62.2		104.0		
			CCSD(T)/DZP[d]	47.8		90.6			56.6		99.4		
			B3LYP/DZP	35.2	36.9	75.6	74.6	352i	47.6	49.7	88.0	87.4	183i
Si	Sn	Ge	HF/DZP	104.5	105.0	116.0	115.6	1014i	94.2	97.6	105.9	108.1	305i
			MP2/DZP	57.5	59.1	72.0	72.3	524i	55.6	59.4	70.0	72.7	260i
			QCISD/DZP[c]	54.4		69.3			52.4		67.4		
			CCSD(T)/DZP[d]	48.5		63.5			47.1		62.2		
			B3LYP/DZP	32.1	33.5	45.8	46.2	318i	37.6	40.6	51.3	53.3	172i
Si	Sn	Sn	HF/DZP	96.5	97.4	122.4	120.9	967i	86.8	90.2	112.7	113.7	295i
			MP2/DZP	50.8	52.4	83.8	83.7	630i	47.4	50.9	80.4	82.2	227i
			QCISD/DZP[c]	47.0		79.9			44.6		77.5		
			CCSD(T)/DZP[d]	41.4		75.3			39.4		73.7		
			B3LYP/DZP	26.5	28.1	58.0	57.3	311i	30.3	33.2	61.8	62.4	140i
Ge	Si	Sn	HF/DZP	106.7	106.9	131.2	129.8	969i	117.4	119.7	141.0	142.6	396i
			MP2/DZP	59.2	59.9	86.8	86.6	574i	72.5	74.9	100.1	101.6	336i
			QCISD/DZP[c]	60.4		87.3			72.5		99.4		
			CCSD(T)/DZP[d]	54.3		82.1			67.0		94.8		
			B3LYP/DZP	39.1	39.7	65.7	64.7	421i	56.2	58.1	82.8	83.1	250i
Ge	Ge	Sn	HF/DZP	106.8	107.0	126.6	125.3	862i	115.4	117.2	135.3	135.5	328i
			MP2/DZP	61.0	61.8	84.2	84.2	495i	73.2	75.1	96.3	97.5	296i
			QCISD/DZP[c]	60.7		83.2			72.1		94.6		
			CCSD(T)/DZP[d]	55.3		78.7			65.3		88.9		
			B3LYP/DZP	41.0	41.6	63.3	62.4	360i	56.9	58.2	79.3	79.0	210i
Ge	Sn	Sn	HF/DZP	100.2	100.2	114.4	113.2	951i	92.0	94.0	106.3	107.0	254i
			MP2/DZP	56.1	56.7	74.6	74.7	546i	54.8	57.2	73.3	75.2	229i
			QCISD/DZP[c]	53.8		71.7			52.6		70.6		
			CCSD(T)/DZP[d]	48.3		67.4			47.6		66.5		
			B3LYP/DZP	31.8	32.5	52.6	52.0	312i	37.9	39.7	55.7	56.3	147i

[a] Energies in kJ mol^{-1}. [b] Frequencies in cm^{-1}. [c] QCISD/DZP//MP2/DZP. [d] CCSD(T)/DZP//MP2/DZP.

Downloaded by CARLI CONSORTIUM on June 29, 2009
Published on March 3, 2000 on http://pubs.acs.org | doi: 10.1021/om990886j

mental interest, that either or both mechanisms might be in operation.

Reactions Involving Methyl Radical. Extensive searching of the C_2H_9Z (Z = Si, Ge, Sn) potential energy surfaces located transition states **6** for the degenerate frontside attack of methyl radical at the heteroatom in methylsilane, methylgermane, and methylstannane at uncorrelated levels of theory (Scheme 2; Y = C). When MP2/6-311G** or MP2/DZP was used, structures **6** (Y = C, Z = Si, Ge) collapsed to the transition states **9**

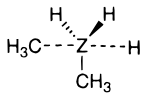

9 (Z = Si, Ge)

for expulsion of hydrogen atom by the backside mechanism. Similar results were obtained for the silicon-containing system at the MP2/cc-pVDZ and MP2/aug-cc-pVDZ levels of theory. Only the tin-containing transition state **6** (Y = C, Z = Sn) could be located at a correlated (MP2/DZP) level of theory.

Structures **6** (Y = C) are displayed in Figure 2, while calculated energy barriers ($\Delta E^{\ddagger}$, Scheme 2) are listed in Table 6. Included in Table 6 are previously calculated data[17] for the analogous backside attack mechanism involving transition state **5**. Given our failure to locate structures **6** (Y = C, Z = Si, Ge) at correlated levels of theory, it seems highly likely that reactions involving silicon and germanium do not have a frontside mechanism available for homolytic substitution by methyl radical. The reaction at tin, however, is predicted to proceed by both pathways, and as observed for the other systems in this study, both mechanisms would appear to have similar energy requirements, with QCISD/DZP//MP2/DZP energy barriers of 86.9 and 89.2 kJ mol^{-1} for reactions involving **5** and **6**, respectively.

The failure to locate frontside transition structures **6** at the MP2 level of theory for attack at silicon and germanium is not surprising. Previous MP2/DZP cal-

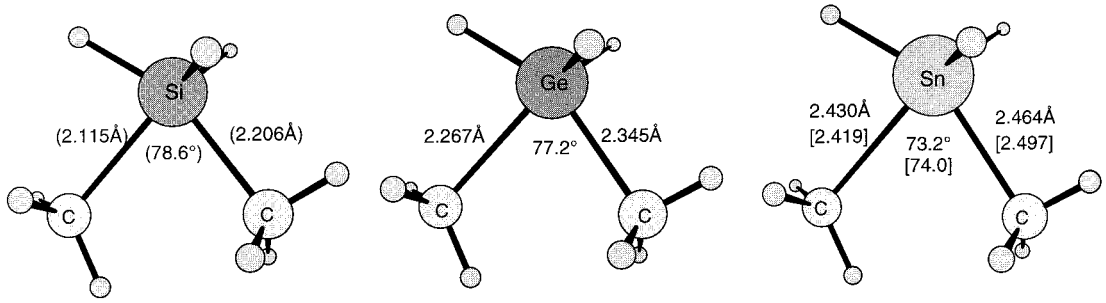

Figure 2. Available UHF/DZP optimized structures of transition states **6** involved in the degenerate frontside reaction of methyl radical with methylsilane ($MeSiH_3$), methylgermane ($MeGeH_3$), and methylstannane ($MeSnH_3$). UHF/6-311G** data are given in parentheses and MP2/DZP data in brackets.

Table 6. Calculated Energy Barriers[a] ($\Delta E^{\ddagger}$) for the Degenerate Reactions of Methyl Radical with Methylsilane, Methylgermane, and Methylstannane (Scheme 2; Y = C, Z = Si, Ge, Sn) and Transition State (Imaginary) Frequencies (ν)[b] of Structures 6

			6			**5**[c]
Y	Z	method	$\Delta E^{\ddagger}$	$\Delta E^{\ddagger}$ + ZPE	ν	$\Delta E^{\ddagger}$
C	Si	HF/6−311G**	190.4	203.7	815i	184.2
		HF/DZP				182.7
C	Ge	HF/DZP	178.1	189.1	678i	173.4
C	Sn	HF/DZP	136.7	146.9	598i	152.6
		MP2/DZP	96.6	107.1	563i	92.0
		QCISD/DZP//MP2/DZP	89.2			86.9
		CCSD(T)/DZP//MP2/DZP	82.2			
		B3LYP/DZP	62.5	70.3	293i	

[a] Energies in kJ mol^{-1}. [b] Frequencies in cm^{-1}. [c] Taken from ref 17.

culations revealed that the structures **5** (Y = C) involved in the backside homolytic substitution mechanism at silicon, germanium, and tin correspond to hypervalent intermediates which are constrained by low barriers to dissociation.[17] If intermediates exist in these reactions, then it seems likely that structures **6** (Y = Si, Ge), which would require only a 10° deviation in geometry to become T-shaped, may well not exist on the MP2 potential energy surfaces.

Acknowledgment. The support of the Australian Research Council and the Melbourne Advanced Research Computing Center is gratefully acknowledged. We also thank Dr. Chryssostomos Chatgilialoglu for stimulating discussion.

Supporting Information Available: Gaussian archive entries for all calculations in this study. This material is available free of charge via the Internet at http://pubs.acs.org.

OM990886J

Downloaded by CARLI CONSORTIUM on June 29, 2009
Published on March 3, 2000 on http://pubs.acs.org | doi: 10.1021/om990886j